



1 **Seiche excitation in a highly stratified fjord of southern**  
2 **Chile: the Reloncaví fjord.**

3

4

5 Manuel I. Castillo<sup>1\*</sup>, Oscar Pizarro<sup>2,3,4</sup>, Nadin Ramírez<sup>2,4</sup> and Mario Cáceres<sup>1</sup>

6

7

8 [1] {Facultad de Ciencias del Mar y Recursos Naturales, Universidad de Valparaíso,

9 Valparaíso, Chile.}

10 [2] {Programa COPAS-Sur Austral, Universidad de Concepción, Concepción, Chile.}

11 [3] {Departamento de Geofísica, Universidad de Concepción, Concepción, Chile.}

12 [4] {Instituto Milenio de Oceanografía, Universidad de Concepción, Chile.}

13

14

15

16

17

18

19 \*Correspondence to: [manuel.castillo@uv.cl](mailto:manuel.castillo@uv.cl)

20

21



1 **Abstract**

2  
3 We describe a seiche process in a Chilean fjord, based on current, temperature and sealevel  
4 data obtained from the Reloncavi fjord (41.6° S, 72.5° W) in southern Chile. We combined  
5 four months of ADCP data with sealevel, temperature and wind time series to analyze the  
6 dynamics of low-frequency (periods > 1 day) internal oscillations in the fjord. Additionally,  
7 seasonal CTD data from 19 along-fjord stations were used to characterize the seasonality of  
8 the density field. The density profiles were used to estimate the internal long-wave phase  
9 speed ( $c$ ) using two approximations: (1) a simple reduced gravity model (RGM) and (2) a  
10 continuously stratified model (CSM). No major seasonal changes in  $c$  were observed using  
11 either approximation (e.g., the CSM yielded  $0.73 < c < 0.87$  m s<sup>-1</sup> for mode 1). The natural  
12 internal periods ( $T_N$ ) were estimated using Merians's formula for a simple fjord-like basin  
13 and the above phase speeds. Estimated values of  $T_N$  varied between 2.9 and 3.5 days and  
14 were highly consistent with spectral peaks observed in the along-fjord currents and  
15 temperature time series. We conclude that these oscillations were forced by the wind stress,  
16 despite the moderate wind energy. Wind conditions at the end of winter gave us an excellent  
17 opportunity to explore the damping process. The observed damping time ( $T_d$ ) was relatively  
18 long ( $T_d=9.1$  days).

19

20 **1 Introduction**

21

22 Internal seiche oscillation has long been known in closed basin geometries (e.g. Watson  
23 1904; Wedderburn 1907; Wedderburn and Young 1915). The first detailed description  
24 thereof was presented by Mortimer (1952). In these systems, wind is the main force affecting  
25 the surface and isotherms (Wiegand and Chamberlain, 1987), which produces a set of  
26 periodic oscillations and circulation cells throughout the water column that may contribute to  
27 internal mixing of the basin (Thorpe 1974; Monismith 1985; Wiegand and Chamberlain  
28 1987; Munnich et al. 1992; Mans et al. 2011; Simpson et al. 2011).

29

30 Although external (barotropic) seiches are ubiquitous in closed basin geometries (Munnich et  
31 al. 1992), it is not theoretically evident that there are internal seiches (baroclinic) in a linearly  
32 stratified fluid (Maas and Lam 1995). It is possible to find resonant basin modes only in



1 well-behaved geometries (Arneborg and Liljebladh, 2001a).. However, studies of lakes have  
2 yielded good results using layered models (e.g. Lemmin 1987), normal-mode approximations  
3 (e.g. Wiegand and Chamberlain 1987; Münnich et al. 1992) or numerical model simulations  
4 (e.g. Goudsmit et al. 2002). In fact, internal seiches have been observed in semi-enclosed  
5 systems such as fjords (e.g. Djurfeldt 1987; Pasmara and Stigebrandt 1997; Arneborg and  
6 Liljebladh, 2001a) with complex geometries and where linear stratification is rarely  
7 observed, and thus the only way to maintain consistency with the theory is that the  
8 oscillation on the pycnocline dominates the internal seiche oscillation (Arneborg and  
9 Liljebladh, 2001a). Early in the development of a seiche, its amplitude is related to the  
10 forcing intensity, and the standing oscillation then becomes free and requires no additional  
11 forcing. The frequencies are retained, but the amplitudes decays (damping) exponentially due  
12 to friction until the system comes to rest (Rabinovich 2010). The development of seiche  
13 oscillations depends of the forcing and damping mechanisms; with large damping, it is  
14 impossible to observe a seiche, whereas small damping of a seiche allows for several  
15 oscillations (Arneborg and Liljebladh, 2001a).

16

17 In fjords with shallow sills, the interaction between the sill and the barotropic tide generates  
18 internal tides that are more energetic than other internal oscillations and are the focus of most  
19 studies regarding mixing and internal oscillations based on internal tides (e.g. Stigebrandt  
20 1980; Stigebrandt and Aure 1989; Inall and Rippeth 2002; Ross et al. 2014). In the case of  
21 fjords with a deep sill and low tidal energy, the breaking of the internal seiche oscillations at  
22 the boundaries could be an important contributor to the internal mixing, promoting the  
23 spreading of properties within the fjord, particularly in deep waters (Stigebrandt and Aure  
24 1989; Münnich et al. 1992; Arneborg and Liljebladh 2001b). Additionally, there are  
25 evidences that vertical isopycnal displacements in fjords could be generated by similar  
26 displacements outside the fjord (e.g. Svensen 1980; Djurfeldt 1987). These remotely  
27 generated oscillations could enhance the mixing and ventilation in deep fjords.

28

29 There is still only limited understanding of the main oceanographic processes occurring in  
30 the fjord region of southern Chile, although there has been local research during the previous  
31 few decades. Since early studies of the hydrography by Pickard (1971), a systematic



1 measurement program in the fjord region has been maintained since 1995 (Palma and Silva  
2 2008; Pantoja et al. 2011; Iriarte et al. 2014), although only a small number of studies have  
3 focused on the physical dynamics. Most studies have been conducted over short time spans  
4 (e.g. Cáceres et al. 2004; Valle-Levinson et al. 2007), and only a few studies have been based  
5 on more than one month of data (e.g. Valle-Levinson and Blanco 2007; Letelier et al. 2011;  
6 Castillo et al. 2012; Schneider et al. 2014), thereby limiting our understanding of sub-inertial  
7 variability. In the Reloncavi fjord, time series of approximately 4 months have shown  
8 evidence that 3-day oscillations of currents could be produced by internal seiche oscillations  
9 (Castillo et al., 2012) but lack on the forcing to describe the forcing mechanism and the  
10 seasonal modulation.

11

12 This study presents the first evidence of internal seiche oscillations in a fjord in southern  
13 Chile. The objective of this study was to address the following questions: How do these  
14 oscillations affect the temporal and spatial dynamics of currents and temperature? How are  
15 these oscillations forced?

16

## 17 **2 Study area**

18

19 The Reloncavi fjord (41.5°S, 72.5°W) is the northern most fjords on the coast of Chile (Fig.  
20 1). This "J" shaped fjord is 55 km long and has a width that varies from 3 km near the mouth  
21 to 1 km near the head. There is a deep sill (~ 200 m depth) located 15 km inland although it  
22 does not appear to be a barrier to the exchange of properties between the adjacent basins.  
23 Based on bathymetric features and the coastline morphology, this fjord can be separated into  
24 four sub-basins displaying the characteristics presented in Table 1 and figure 2.

25

26 The main river discharge is provided by the Puelo River (at the middle of the fjord), which  
27 produces a mean annual discharge of  $650 \text{ m}^3 \text{ s}^{-1}$ . The Petrohue River (at the head of the fjord)  
28 has an mean annual discharge of  $255 \text{ m}^3 \text{ s}^{-1}$ , and there are additional freshwater inputs of  
29 minor importance compared with the Cochamo river (mean annual discharge of  $20 \text{ m}^3 \text{ s}^{-1}$ )  
30 and Canutillar hydroelectrical plant (mean annual discharge  $75.5 \text{ m}^3 \text{ s}^{-1}$ ) (Niemeyer and  
31 Cereceda, 1984). The freshwater input to the fjord due to direct precipitation is only



1 approximately 2% of the main river discharge (León-Muñoz, 2013), and its contribution may  
2 be in balance with evaporation (Castillo et al., 2016). The freshwater input creates a marked  
3 along-fjord pycnocline that is deeper at the head (~8 m) and shallower at the mouth (~3 m)  
4 (Fig. 2).

5  
6 During the winter, the mean wind stress ( $\tau$ ) is low due to calms winds ( $< 10^{-3} \text{ N m}^{-2}$ ). During  
7 storm events in winter,  $\tau$  can reach values as high as  $0.4 \text{ N m}^{-2}$  (winds of  $> 10 \text{ m s}^{-1}$ ), and the  
8 wind tends to blow out of the fjord, thereby reinforcing the upper outflow of brackish water.  
9 In contrast, during the spring/summer, the winds exhibit a marked diurnal cycle, and  $\tau$  can  
10 reach values as high as those observed in the winter, whereas the wind blows landward, i.e.,  
11 toward the fjord's head and against the upper flow. Tides in the Reloncavi fjord are  
12 predominantly semi-diurnal, and during spring tidal range never exceed 6 m, whereas the  
13 neap tidal range is about 2 m. The tidal current is relatively weak in the upper layer, which is  
14 dominated by gravitational circulation (Valle-Levinson et al., 2007; Montero et al., 2011;  
15 Castillo et al. 2012).

16

### 17 **3 Data and Methods**

18

#### 19 **3.1 Field Observations**

20

21 Current measurements were obtained using Teledyne RD Instruments Acoustic Doppler  
22 Currentmeter Profilers (ADCPs) in three subsurface mooring systems. These subsurface  
23 systems were located near the fjord mouth, near the Puelo River and between the Cochamo  
24 and Petrohue Rivers (Fig. 1). The longest time series spanned the period of August through  
25 November 2008 (Fig. 1 and Table 1). At the mouth, two upper-looking ADCPs were  
26 positioned at nominal depths of 10 m (300 kHz) and 450 m (75 kHz). The Puelo mooring  
27 held two ADCPs, one facing-up at a depth of 30 m (600 kHz) and one facing downward at a  
28 depth of 35 m (300 kHz). The Cochamo mooring held one facing-up ADCP at a depth of 11  
29 m (300 kHz). Note that due to the large tidal range, the depths of the ADCPs significantly  
30 changed with the tides. These effects — along with small vertical deviations of the ADCPs  
31 related to the line movements — were corrected using the ADCPs pressure sensors, and all  
32 of the bin depths were referenced to the water surface level. The mooring systems were



1 designed to obtain the best vertical resolution available with emphasis on the upper layer.  
2 The ADCP cell sizes were 0.5 m (600 kHz), 1 m (300 kHz) and 4 m (75 kHz), and the data-  
3 acquisition time intervals were 10 minutes in most of the ADCPs, with the exception of the  
4 deepest ADCP, which was set to acquire data at an interval of 20 minutes. All the ADCPs  
5 configurations maintain a standard deviation  $< 2 \text{ cm s}^{-1}$  (details in supporting information  
6 S2).

7  
8 The morphology of the fjord exhibits a sharp bend in the middle, and thus the  $x$  and  $y$ -  
9 components of the currents were rotated to the local orientation of the along-fjord axis (Fig.  
10 1 and Table 1). A right-handed coordinate system with a positive-up  $z$ -axis and an along-  
11 fjord  $y$ -axis (positive toward the fjord head) was used. Consequently, the cross-fjord  $x$ -  
12 component was positive toward the south (east) near the fjord mouth (head). To assess the  
13 contribution of the tides to the currents, the amplitudes and phases of several tidal  
14 components were calculated at all of the moored ADCPs using a standard harmonic analysis  
15 from Pawlowicz et al. (2002).

16  
17 The vertical structure of the temperature was obtained from Onset HOBO-U22 temperature  
18 sensors installed in three mooring systems along the fjord (Fig. 1). These moorings held  
19 surface buoys supporting the thermistor chains with an anchor located at a 25 m depth to  
20 maintain their nominal depths (0, 1, 2, 3, 4, 5, 7, 9, 11, 13, 15 and 20 m) from the surface  
21 independent of tidal fluctuations. Temperature data were collected every 10 minutes at all  
22 locations.

23  
24 A Davis Vantage Pro2 meteorological station was installed south of the Puelo River (see Fig.  
25 1). This station held sensors for measuring the wind direction and velocity, solar radiation,  
26 rain, and air temperature. The wind magnitude and direction sensors were installed 10 m  
27 above sealevel and were set to collect data every 10 minutes from 12 June 2008 to 30 March  
28 2011. Gaps in the time series represented only 0.04% of the total data. The wind stress ( $\tau$ )  
29 was calculated using a drag coefficient dependent on the magnitude (see Large and Pond,  
30 1981) and a constant air density of  $1.2 \text{ kgm}^{-3}$ .

31



1 The salinity and temperature profiles were obtained seasonally using a CTD SeaBird SBE 25  
2 at 19 stations in the along-fjord transect shown on Figure 1. The data were processed  
3 following the standard protocol suggested by the manufacturer and were averaged in vertical  
4 intervals of 0.5 m. Due to large salinity changes in the upper layer, the instrument pump was  
5 set to a time interval of 1 minute. After the start of the pumping, the instrument was  
6 maintained near the surface until the sensors stabilization. Then, the CTD was lowered to the  
7 maximum depth of the station (Table 2). The along-fjord transects typically required 12 to 24  
8 hours to complete, depending on local weather conditions. Due to technical limitations, the  
9 winter transect was performed to a maximum depth of 50 m.

10

11 The sealevel was recorded every 10 minutes using two pressure sensors moored over the  
12 seabed. At Cochamo, the pressure sensor was an Onset HOBO-U20, whereas a SeaBird  
13 wave-tide gauge SBE-26 was installed near the fjord's mouth (Fig. 1). Subsurface pressure  
14 data were corrected for air pressure and converted to an adjusted sealevel.

15

16 Discharge data were provided by Dirección General de Aguas, Chile (Dirección General de  
17 Aguas, 2016). These data are regularly collected at a station located 12 km upstream of the  
18 Puelo River's mouth (Fig. 1). The time series extended from January 2003 to December  
19 2011, and data gaps represented only 2% of the total.

20

### 21 **3.2 Time series analysis**

22

23 Previous findings (Castillo et al., 2012) have shown an important oscillation with a period of  
24 approximately 3 days (72 h). To focus the study on these perturbations, we used a cosine-  
25 Lanczos band-pass filter with half amplitudes at 60 h and 100 h (see results for the  
26 justification of the selected band). As part of the results, the band-passed time series of the  
27 current and temperature data are shown (COPAS-SUR Austral, 2012).

28

29 Spectral analyses of the current, wind stress, sealevel and temperature time series were  
30 performed using Welch's modified average periodograms (Emery and Thomson 1998). To  
31 achieve statistical reliability of the spectral estimations, each time series was divided into  
32 non-overlapping segments to generate spectral estimates. In the case of the current time



1 series, the spectra were (additionally) averaged among depth layers to obtain 12, 24 and 48  
2 degrees of freedom, depending on the frequency (see Fig. 3). In addition, to evaluate the  
3 consistency of the periodicity between the time series, we calculate a Morlet cross-wavelet  
4 analysis following wavelet methods explained by (Torrence and Compo, 1998) and (Grinsted  
5 et al., 2004).

6

7 The phase velocity ( $c$ ) was estimated using two models that took into account the fjord  
8 stratification: (1) a simple reduced-gravity model (RGM) and (2) a continuously stratified  
9 model (CSM).

10

11 The reduced-gravity model was developed using the typical density profiles in each sub-  
12 basin. Here, the base of the upper layer was estimated from the pycnocline depth (Fig. 2),  
13 which in the Reloncavi fjord is well represented by the depth of the 24 isohaline ( $h_l$ )  
14 (Castillo et al., 2016), considering that  $h_l$  is the pycnocline depth and  $H$  is the deepest CTD  
15 cast (mostly near to the sub-basins maximum depths). The mean density of the upper layer ( $\rho_1$ )  
16 was estimated from depths between the surface to  $h_l$ , whereas the mean density for the  
17 deep layer ( $\rho_2$ ) was estimated for depths between  $h_l$  and  $H$ . These estimations were made  
18 for each sub-basins, and seasons (Table 2).

19

20 Using both densities,  $\rho_1$  and  $\rho_2$ , the reduced gravity ( $g' = g(\rho_2 - \rho_1) / \rho_2$ ) was obtained,  
21 here  $g$  is the acceleration of gravity. The internal phase velocity of each sub-basin,

22  $c_i = (g' h_{li})^{1/2}$ , where  $i = 1$  to 4 and  $h_{li}$  represents the mean depth of the upper layer in the  
23 sub-basin “ $i$ ” was used to estimate a mean wave speed in the entire fjord,

$$24 \quad T = \frac{L}{c} = \sum_{i=1}^n \frac{L_i}{c_i} \quad (1)$$

25 where  $L_i$  is the  $i$  sub-basin length and  $L$  is the fjord length.

26

27 The continuously stratified model (CSM) was developed using the normal mode analysis,  
28 which introduced the stratification as  $N^2 = -(g / \rho)(\partial\rho / \partial z)$ , which is the buoyancy  
29 frequency, in the Sturm-Liouville expression





$$1 \quad \frac{d}{dz} \left( \frac{1}{N^2} \frac{d\psi_n}{dz} \right) + \frac{1}{c_n^2} \psi_n = 0 \quad (2)$$

2 where  $\psi_n(z)$  is the vertical structure of the horizontal velocity for the mode  $n$ . Here  $c_n$   
 3 represents the  $n$  mode speed (see Gill, 1982) and differs significantly from phase speed if  
 4 rotation plays a role (van der Lee and Umlauf, 2011).

5

6 Independent of the model used to obtain the phase speed (RGM or CSM), the natural  
 7 oscillation period ( $T_N$ ) was determined using Merian's formula for a semi-enclosed basin, as  
 8 suggested by Ravinovich (2010),  $T_N = 4 T$ .

9

10 The modal decomposition was used to obtain the contribution of each mode in the currents  
 11 variability (e.g. Emery and Thomson, 1998; Gill, 1982; van der Lee and Umlauf, 2011). The  
 12 along- and cross-fjord band-pass currents  $[u_{bp}, v_{bp}]$  could be described by the vertical modes  
 13 by (3),

$$14 \quad [u_{bp}, v_{bp}](z, t) = \sum_{n=1}^{\infty} [u_{pj}, v_{pj}](t) \psi_n(z) \quad (3)$$

15

16 The along- and cross-fjord currents projected ( $u_{pj}, v_{pj}$ ) on the vertical modal structure ( $\psi_n$ )  
 was obtained by eq. (4),

$$17 \quad [u_{pj}, v_{pj}](t) = \frac{1}{H} \int_{-H}^0 [u_{bp}, v_{bp}](z, t) \psi_n(z) dz \quad (4)$$

18



1 **4. Results**

2

3 **4.1 Density structure**

4 As a result of abundant freshwater input to the fjord, there were marked differences in  
5 density between the upper and lower layers along the fjord and small changes in stratification  
6 among seasons, particularly near the mouth of the fjord (Fig. 2). One important characteristic  
7 of the upper layer is its high and persistent stratification from the surface to the base of the  
8 pycnocline (Fig. 2). Along the fjord, the pycnocline depth exhibited clear deepening from 2.3  
9  $\pm 0.1$  m at the mouth to  $6.1 \pm 0.3$  m near the head. The pycnocline depth exhibited greater  
10 seasonal variability near the head of the fjord (Fig. 2).

11

12 **4.2 Winds, sealevel and freshwater discharge**

13

14 The along-fjord wind stress ( $\tau$ ) displayed two patterns during the transition from winter to  
15 spring. During the winter,  $\tau$  was generally out of the fjord ( $-0.4 \pm 3 \times 10^{-2}$  N m<sup>-2</sup>) and  
16 displayed oscillations with a period longer than 1 day. There were also strong events ( $> 0.2$   
17 N m<sup>-2</sup>) during the first half of August 2008 that could be associated with the end of winter  
18 storms in the region. This winter pattern drastically changed during the early spring (first  
19 week of September 2008) and was maintained throughout the rest of the season. Changes  
20 were evident in a marked daily cycle and in switches from down- to up-fjord (average of  $1.6$   
21  $\pm 3 \times 10^{-2}$  N m<sup>-2</sup>), against the upper layer outflow (Fig. 3a).

22

23 The sealevel was measured at the mouth and near Cochamo (Fig. 1). At both stations, the  
24 form factor was 0.12, which indicates that semi-diurnal tides dominate in the region. In fact,  
25 the M<sub>2</sub> amplitude was  $1.89 \pm 0.06$  m at the mouth and  $1.91 \pm 0.06$  m near Cochamo. The  
26 mouth-to-head phase difference in this harmonic was negative ( $-2.4^\circ$ ), indicating propagation  
27 toward the head with a lag of approximately 5 minutes. The maximum tidal range during  
28 spring tides was approximately 6 m and less than 1 m during neap tides (Fig. 3b). Similar  
29 ranges have been observed outside the fjord in the Reloncavi sound (Aiken, 2008).

30



1 Discharge was greatest (approximately  $1413 \text{ m}^3 \text{ s}^{-1}$ ) at the end of August 2008 (winter) and  
2 lowers (approximately  $459 \text{ m}^3 \text{ s}^{-1}$ ) at the end of October (spring). In the winter, the historical  
3 mean of  $650 \text{ m}^3 \text{ s}^{-1}$  (Niemeyer and Cereceda 1984; Leon et al 2013) was exceeded 86% of  
4 the time, whereas during the spring, this exceedance occurred only 18% of the time. In fact,  
5 only a small variability around the mean was observed during the spring (Fig. 3c).

6

### 7 **4.3 Along-fjord currents**

8

9 The along-fjord currents were one order of magnitude larger than the cross-fjord currents (in  
10 this study we focused on the along-fjord component). At the three measurements sites at  
11 Cochamo (Fig. 3d), Puelo (Fig. 3e) and the mouth (Fig. 3f), the along-fjord currents  
12 displayed certain common features: (1) semi-diurnal oscillations attributed to tidal effect, (2)  
13 a two layered structure with persistent outflow above the pycnocline and an intermittent  
14 lower inflow layer beneath, and (3) several low-frequency (period  $> 1$  day) oscillations were  
15 present in the time series.

16

17 Currents in the upper outflow layer displayed a mean velocity of  $66 \text{ cm s}^{-1}$  at the mouth and  
18  $45 \text{ cm s}^{-1}$  at Cochamo, indicating that the outflow increased through the mouth. Additionally,  
19 the upper layer was deeper at Cochamo (Fig. 3d) than at the mouth (Fig. 3f), which is  
20 consistent with the along-fjord pycnocline depth (Fig. 2). Below the upper layer, a sub-  
21 surface layer displayed intermittent inflow (see Fig. 3d, 3e and 3f) with a maximum ( $> 20 \text{ cm}$   
22  $\text{s}^{-1}$ ) centered at the  $\sim 6 \text{ m}$  depth.

23

24 This two-layered pattern was clearly observed in the upper 10-15 m and is consistent with a  
25 gravitational circulation due to the along-fjord pressure gradient. This pressure gradient is  
26 also consistent with the observed along-fjord pycnocline tilt (Fig. 2). At depths  $> 20 \text{ m}$ , the  
27 along-fjord currents at Puelo and at the mouth exhibited an important influence ( $> 40\%$  of  
28 the variability) of a semi-diurnal component of the tide. In addition, in this layer, low-  
29 frequency (periods  $> 7$  days) oscillations suggest a bottom-to-surface propagation that was  
30 more intense from the end of August to the beginning of September during a period of high



1 discharge ( $> 650 \text{ m}^3 \text{ s}^{-1}$ ). This layer on average exhibited a weak outflow ( $\sim 1 \text{ cm s}^{-1}$ ) at the  
2 mouth, which in turn implies a 3-layer pattern of the residual flow near the mouth.

#### 4 **4.4 Spectral characteristics of currents, temperature, sealevel and winds**

5  
6 To obtain better statistic reliability, the spectra of the along-fjord currents were depth-  
7 averaged. The upper layer was defined until the pycnocline depth ( $z \leq h_I$ ), whereas the deep  
8 layer contains  $z > h_I$  (Fig. 4).

9  
10 All of the spectra displayed an energetic peak at the semi-diurnal frequency ( $M_2$ ), and this  
11 peak was greater in the deep layer (Fig. 4). In the diurnal band, the spectra at Puelo and at the  
12 mouth presented a clear (and highly energetic) peak in the surface layers. This diurnal peak  
13 is likely due to the influence of wind stress (see Fig. S1), which displayed a marked diurnal  
14 cycle during the late winter (end of August) and spring (Fig. 3a). An important peak ( $10^4 \text{ cm}^2$   
15  $\text{s}^{-2} \text{ cph}^{-1}$ ) was observed only at Cochamo in the 6 hour band ( $M_4$ ), suggesting an increase in  
16 the importance of non-linear interaction between  $M_2$  and the bathymetry in this sub-basin.  
17 The spectra in the upper layer displayed an important accumulation of energy in the band  
18 centered on the 3 days period. The band was wider (between 2 and 7 days) at the mouth and  
19 Puelo and narrower (between 1.5 and 4 days) at Cochamo. At the mouth, the maximum  
20 spectral density was in the 3 days band ( $> 10^5 \text{ cm}^2 \text{ s}^{-2} \text{ cph}^{-1}$ ) and was one order greater than  
21 the maximum spectral density observed at Cochamo ( $\sim 10^4 \text{ cm}^2 \text{ s}^{-2} \text{ cph}^{-1}$ ). Another important  
22 accumulation of energy in the along-fjord currents was centered on the 15 days period. One  
23 characteristic of the 15 days band is the influence on the entire water column at Puelo and the  
24 mouth (Fig. 4).

25  
26 The sealevels at Cochamo ( $\eta_C$ ) and at the mouth ( $\eta_m$ ) were similar at frequencies less than  
27  $0.165 \text{ cph}$  (periods longer than 6 h). The spectra displayed an important accumulation in the  
28 synoptic band (10 days). Both locations exhibited the same energy at the diurnal ( $K_1$ )  
29 semidiurnal ( $M_2$ ) frequencies, although  $M_2$  was clearly the dominant harmonic in the fjord.  
30 The spectral energy was one order of magnitude higher than the diurnal ( $K_1$ ) harmonics and  
31 three orders of magnitude higher than the quarter-diurnal ( $M_4$ ) harmonics. The spectra



1 exhibited no accumulation of energy in the 3days band, although at high frequencies ( $> 0.5$   
2 cph), an important accumulation of energy was observed in the 1.3h band (between 1.16 h  
3 and 1.56 h) at  $\eta_C$  (Fig. 4).

4

5 The wind stress ( $\tau$ ) indicated that the along-fjord wind stress was significantly higher than  
6 the cross-fjord component. The spectra displayed a marked peak (particularly in the along-  
7 fjord component) in the diurnal band, which is likely due to the sea-breeze phenomenon.  
8 Another interesting feature of the spectrum was the peak in the semi-diurnal frequency,  
9 which was observed in both components. At longer periods ( $> 1$  day), the along-fjord wind  
10 stress displayed an important but not statistically significant peak at 2.8 days, which is highly  
11 consistent with the currents (Fig. 4).

12

#### 13 **4.5 Seasonality of the internal oscillations**

14

15 The density structure on the fjord does not show an upper mixing layer along the seasons;  
16 indeed a continuously stratified upper layer is present along the seasons (Fig. 5). The along-  
17 fjord mean of the pycnocline depth ( $h_I$ ), which was estimated based on salinity/density  
18 gradient, was used to estimate the internal phase velocity ( $c$ ) and the internal period ( $T_N$ ).  
19 Seasonally,  $h_I$  does not change significantly during winter, spring and summer (between 4.6  
20 and 4.8 m) but was shallower during autumn ( $\sim 4.1$  m) (Table 2). In addition, the density  
21 structure showed a condition of continuous stratification in the upper layer along the seasons  
22 (Fig. 5).

23

24 In the case of the RGM approximation, internal phase velocities ( $c$ ) were highest during  
25 spring and summer ( $> 0.83$  m s $^{-1}$ ) whereas in winter and autumn the intensities were  $< 0.76$   
26 m s $^{-1}$ , thus we obtain internal periods between 2.9 and 3.4 days (70 and 82 hours) (Table 2).

27

28 The horizontal velocity structure ( $\psi_n$ ) profile of the first 3 internal modes obtained from the  
29 CSM, showed high consistency along the fjord (in each sub-basin) and through the seasons  
30 (Fig 5). The mode 1 was highly baroclinic changing of sign nearly of 10 m (sub-basin I) and  
31 15 m (sub-basin IV). In the case of mode 2 and 3, relatively high variability along the



1 seasons was observed specially at the sub-basins I and IV above of 20 m depth. For depths >  
2 30 m (not shown) the internal modes do not show significant variability (Fig. 5). The modal  
3 speeds for the first 3 modes described above were relatively high during spring and summer  
4 ( $c_I$  was  $> 0.84 \text{ m s}^{-1}$ ) and lower during winter and autumn (here  $c_I$  was  $< 0.77 \text{ m s}^{-1}$ ). These  
5 results were highly consistent with the internal speeds obtained by RGM (Table 2).

6

7 As the internal speeds ( $c$ ), the natural internal period ( $T_N$ ) obtained by RGM with the mode 1  
8 of CSM were highly consistent. For comparison, we take into account  $T_N$  obtained from the  
9 mode 1 of the CSM which ranged between 2.9 days (spring) and 3.5 days (winter). The  
10 estimations of  $T_N$  with RGM showed speeds between 2.9 days (spring) and 3.4 days (winter  
11 and autumn) in hours this range was between 70 and 84 hours, indicating that oscillations  
12 between these periods are dominated by mode 1 internal seiche oscillation.

13

14 To focus on these internal seiche oscillations, we filtered the along-fjord currents with a 70h  
15 to 90h cosine-Lanczos band-pass filter. Additionally, mode 1 of the internal seiche was  
16 associated with the pycnocline depth, which is restricted to the upper 8 m (Fig. 2). Therefore,  
17 we describe the along-fjord currents in the upper 10 m (Fig. 6).

18

19 Vertical pattern at the three locations shows inflow/outflow intermittence along the whole  
20 time series, also mostly of these along-fjord structures seems to develop an inclination which  
21 suggest the baroclinic nature of this pattern. The band-pass along-fjord currents were intense  
22 at the mouth ( $> 15 \text{ cm s}^{-1}$ ) but diminish toward the head. Intense perturbations oscillations  
23 were observed near the surface between 10 and 20 August 2008 at the mouth and Cochamo,  
24 internal intensification (between 4 m and 10 m depths) of the inflow/outflow pattern was  
25 clear at Puelo and Cochamo at the ends of September. To confirm whether the nature of the  
26 along-fjord currents pattern was baroclinic or barotropic we used  $\psi_n(z)$  to project the band-  
27 pass currents (eq. 3 and 4), similar to van der Lee and Umlauf (2011).

28

29 As an example, for the Cochamo along-fjord currents, the projection using only the mode 1,  
30 represented 44% of the band-pass variability. The use of the first three internal modes  
31 explained the 73% of the variability. Similarly, the barotropic mode only takes into account



1 of the 5% of the variability indicating the baroclinic nature of the band-pass pattern of the  
2 along-fjord currents.

3

4 The projected along-fjord currents (modes 1-3) shows clearly the intensifications at the  
5 surface of the middle of August, and the internal intensification of the ends of September,  
6 also the currents at the mouth were more intense than Cochamo and the complex vertical  
7 structures of the inflow/outflow were well defined by the projections (Fig. 7). In addition,  
8 we estimated the kinetic energy ( $K_E$ ) of the projected along-fjord currents for the first 3  
9 baroclinic modes by,

$$10 \quad K_E = \frac{1}{2} \sum_{n=1}^m (u_{pj}^2 + v_{pj}^2) \quad (5)$$

11 The vertical averaged  $K_E$  at the mouth was higher than Cochamo, here the total  $K_E$  represent  
12 only 9% of the total  $K_E$  at the mouth. The quoted inflow/outflow intensification was also  
13 observed in  $K_E$ . During the August intensification  $K_E$  at Cochamo might be 4% of the mouth,  
14 whereas during September  $K_E$  at Cochamo might be as large as 15% to the mouth (Fig. 7).

15

16 Along-currents were highly coherent at 3 days band which is the period of the first mode of  
17 the internal seiche (Table 2). To describe the variability of this high coherence along the  
18 time, we selected 3 m depth ADCP bins (on the upper layer) from the mouth, Puelo and  
19 Cochamo to make a Morlet cross-wavelet analysis and to estimate the squared coherence  
20 (only refer as coherence hereafter) and phase spectrums for the relations mouth/Puelo (MP)  
21 (Fig. 8b, 8c) and Puelo/Cochamo (PC) (Fig. 8d, 8e). Both relations showed high coherence in  
22 the semi-diurnal and diurnal band especially during spring-tides.

23

24 At the 3 day band, the MP relation shows significant coherence during into the fjord winds  
25 whereas low coherence was observed during the opposite winds (Fig. 8a and 8b). Similarly,  
26 the coherence for the PC relation was high along the 3 days band except during the change of  
27 the wind direction described above (Fig. 8d). The associated phase spectra (only the  
28 significant coherence) at the 3 days band was  $\sim 0^\circ$  indicating that the oscillation is in phase  
29 along the fjord (Fig. 8c and 8e).

30



1 At the beginning of the time series, intense fluctuations were observed at Cochamo and at the  
2 mouth (Fig. 6). To explore their relationship with the wind forcing, a detailed view of the  
3 period between 8 and 31 August 2008, is presented in Fig. 9. During this period, the along-  
4 fjord wind stress (not filtered) displayed three different states: (a) strong ( $> 0.2 \text{ N m}^{-2}$ ) up to  
5 the fjord winds, (b) weak ( $< 0.1 \text{ N m}^{-2}$ ) or nearly calm winds and (c) moderate ( $\sim -0.1 \text{ N m}^{-2}$ )  
6 down to the fjord winds. During (c), the winds displayed an apparent diurnal cycle (e.g.,  
7 Fig. 3a).

8  
9 Although density is dominated by salinity, here we used temperature moorings to emphasize  
10 that the internal oscillation reported here had an expression in other properties of the water  
11 within the fjord. In addition, the band-pass temperature time series and the along-fjord  
12 currents shows consistent oscillations pattern (Fig. 9). During (a), the upper outflows  
13 weakened due to the opposing winds at the surface. This change reached depths consistent  
14 with the pycnocline (Fig. 2), caused a disruption and subsequently forced the internal  
15 oscillations observed in the currents and temperature fields (Fig. 9). Here, intense  
16 perturbations were observed that weakened the surface outflow and introduced the colder  
17 water of the upper layer to depths  $> 2 \text{ m}$  at Cochamo and Puelo. During (b), the upper  
18 outflow displayed minimum perturbations in both the currents and temperature. In (c),  
19 perturbations in the currents and temperature were evident at Cochamo and at the mouth with  
20 no major oscillations at Puelo (Fig. 9).

21

## 22 **5 Discussion**

23

24 We used data from one of the most extensive study ever conducted in a Chilean fjord. The  
25 data included currents (ADCPs) and temperatures from moored instruments, seasonal CTD  
26 information and times series of winds and sealevel to study the dynamics of the internal  
27 seiche oscillations in the Reloncavi fjord.

28

29 In fjords with shallow sills such as the Gullmar fjord in Sweden (Arneborg and Liljebldh,  
30 2001a), the Knight Inlet in Canada (Farmer and Freeland, 1983) and the Aysen fjord in Chile  
31 (Cáceres et al., 2002), internal tide oscillations may play a key role in the internal mixing





1 (e.g. Stigebrandt 1976; Farmer and Smith 1980). In lakes, large internal seiche oscillations  
2 significantly contribute to the mixing of the entire basin (Cossu and Wells, 2013), and these  
3 oscillations could also be important in fjords where the relative importance of internal tides  
4 may be less than the internal seiche oscillations (Arneborg and Liljebladh, 2001b).  
5  
6 In this study, we demonstrate the presence (and persistence) of seiches in a Chilean fjord  
7 based on the sealevel slope (barotropic seiche), currents and temperatures (internal seiche).  
8 We also studied the main processes forcing the natural oscillation of the pycnocline.  
9  
10 At high frequencies, the tidal spectrum (Fig. 5) displayed a clear accumulation of energy  
11 centered at a period of 1.3 h. This frequency is not related to any tidal harmonic interactions  
12 (Pawlowicz et al., 2002), and the shape of the spectrum (it is not a peak) suggests resonance  
13 in this frequency band. We explored the effect of the natural oscillation of the basin in this  
14 pattern using the barotropic phase velocity ( $c$ ) for a shallow water wave  $c = (gh)^{1/2}$ , where  $h$   
15 is the mean depth of the fjord. If one assumes a mean fjord depth of  $h = 250$  m (Table 1),  
16 then  $c = 49.5$  m s<sup>-1</sup>, and the natural period  $T_N = 4L c^{-1} = 1.24$  h. This period is lower than the  
17 observed period in Fig. 5 (1.3 h) because the mean depth takes into account the entire fjord  
18 bottom profile (Fig. 1), and thus the effective depth (up to Cochamo) was 233 m and it is  
19 closer to the 226 m necessary to obtain the observed period in Fig. 5. Winds in the region are  
20 moderate (see Fig. 3), but their intensity is sufficient to tilt the surface slope at Cochamo  
21 (Castillo et al., 2012), and thus the surface of the fjord oscillates with the natural period of  
22 the basin. Further evidence of this pattern is provided by the clear differences in amplitude of  
23 the sealevel spectrum at Cochamo (near the fjord's head) and at the mouth. This association  
24 is attributed to the dynamics of seiches in fjords, which tend to produce a node at the mouth  
25 and an anti-node at the head (Dyer, 1997). At the node, the sealevel amplitude must be zero,  
26 whereas near the head, it must be a maximum. This pattern is highly consistent with the  
27 observed spectra at 1.3 h (Fig. 5). Based on all of these results, we suggest that oscillations  
28 close to 1.3 h will resonate with the natural period along the fjord.  
29  
30 Daily winds were highly coherent with surface along-fjord currents, especially on the  
31 brackish water layer (S1). During the spring, daily periodicity of winds was strong (Castillo



1 et al., 2016) with intensities capable of perturb the pycnocline and to induce the internal  
2 seiching process.

3

4 The surface slope indicates that the sealevel at Cochamo was 0.07 m higher than at the  
5 mouth, and this value can be taken as the amplitude of the surface seiche. According to the  
6 RGM, the pycnocline deviation ( $\eta_l$ ) is related to the surface elevation ( $\eta_0$ ) in the form  
7  $\eta_l = -(\rho / \Delta\rho) \eta_0$ , which implies that for a mean surface perturbation of 0.07 m and a  
8 typical  $\Delta\rho$  of  $15 \text{ kg m}^{-3}$ , we obtain a mean  $\eta_l$  of -4.8 m. This finding indicates that the water  
9 piles up at the head of the fjord, likely due to the predominant into the fjord winds in the  
10 region (Fig. 3a) and produces a pycnocline deepening of about 5 m (Fig. 2).

11

12 At low frequencies (periods > 1 day), the along-fjord currents spectra displayed a marked  
13 peak in energy centered at 3 days. To explore the origin of this variability, we analyzed the  
14 density profiles along the fjord (Fig. 2) and applied two methods, the RGM and CSM. The  
15 internal phase velocities ( $c$ ) obtained from both methods were similar, and ranged between  
16  $0.73 \text{ m s}^{-1}$  and  $0.87 \text{ m s}^{-1}$  (taking into account the mode 1 of CSM for comparison). The high  
17  $c$  value was obtained during the spring (November 2008), when the upper layer presented the  
18 lowest densities of the seasons, likely due to high discharge ( $> 1000 \text{ m}^3 \text{ s}^{-1}$ ). Remarkably, the  
19 stratification is linked to the freshwater input despite no major observed changes in  $c$  (Fig.  
20 6e-h). The high consistency between the CSM (mode 1) modal speeds and the phase speed  
21 obtained by RGM suggest that rotation do not play a significant role on the along-fjord  
22 dynamics of these oscillations (van der Lee and Umlauf, 2011). But cross-fjord, the  
23 dynamics has been nearly geostrophic, especially at the fjord's mouth (Castillo et al., 2012).

24

25 For longer periods (> 10 days), there are evidences of baroclinic oscillations clearly observed  
26 on the along-fjord time series (Fig. 3) and in the averaged spectra (Fig. 4). Recently, Ross et  
27 al. (2015), described a similar periodicity on currents of a southern Patagonian fjord of Chile  
28 associated to Baroclinic Annular variability, a regional feature on the air-pressure in the  
29 region. This mechanism of generation for the 10 days oscillations on the Reloncavi fjord  
30 needs to be verified on future studies.

31



1 The internal  $T_N$  of the entire fjord displayed periods between 2.9 and 3.5 days. These results  
 2 suggest that the accumulation of energy observed in the along-fjord currents are due to the  
 3 first mode of an internal seiche oscillation in the fjord. This result could be explained by the  
 4 presence of a node at the mouth, where the sealevel amplitude is minimum (Fig. 5) but the  
 5 currents are maxima (Figs. 3 and 6). This difference was also observed in the projected  
 6 currents ( $u_{pj}$ ,  $v_{pj}$ ) supporting the idea of the presence stationary wave along the fjord.  
 7 Additionally, the currents were highly coherent and in phase (Fig. 8) as we expected from a  
 8 basin-scale seiche wave like. As a way of estimate the contribution of the internal seiche to  
 9 the internal mixing the  $K_E$  was enhanced during the into the fjord winds (Figs. 3 and 7),  
 10 which were periods when the internal seiche band (3 days) was highly coherent along the  
 11 fjord (Fig. 8).

12

13 The winds exhibited high coherence with the along-fjord currents until the pycnocline  
 14 depths, at frequencies centered at 1 and 3 days (see Fig. S1). To study the extent to which the  
 15 wind stress perturbs the pycnocline, we used the Wedderburn number, which is given by the  
 16 equation  $W = (h_1 / L) Ri$  (Thompson and Imberger, 1980; Monismith, 1986), where

17  $Ri = g'(h_1 / u_*^2)$  represents the bulk Richardson number, an index of the stability of the upper  
 18 layer ( $h_1$ ). The frictional velocity ( $u_*$ ) is obtained from the surface wind stress using the  
 19 equation  $u_*^2 = \tau / \rho_0$ , which results in the equation,

$$20 \quad W = \frac{h_1^2 \Delta \rho g}{L \tau} \quad (6)$$

21

22 According to Thompson and Imberger (1980), this value indicates the effect of the wind  
 23 stress on local upwelling in a stratified fluid (i.e., perturbing the pycnocline). Under weak  $\tau$   
 24 conditions ( $W \gg 1$ ), the wind energy is insufficient to tilt the interface. Under strong  $\tau$   
 25 conditions ( $W \ll 1$ ), however, upwelling conditions dominate, there by tilting the interface,  
 26 which produces conditions favorable to forcing of the internal seiche. The critical conditions  
 27 ( $W \sim 1$ ) indicate the beginning of upwelling (Thompson and Imberger, 1980; Stevens and  
 28 Imberger, 1996), although the ideal transition point occurs at  $W = 0.5$  (Monismith, 1986). All  
 29 of these conditions were observed during the period of August 2008, as it is shown on Fig. 9.



1 During strong  $\tau$  ( $\sim 0.3 \text{ N m}^{-2}$ ) conditions,  $W = 0.27$  produced intense perturbation of the  
2 pycnocline (Fig. 9a). In contrast, during weak  $\tau$  ( $\sim 0.01 \text{ N m}^{-2}$ ) conditions, a value of  $W = 8$   
3 indicates that the wind was too weak to perturb the pycnocline, favoring a seiche damping  
4 process (Fig. 9b). Transition conditions occurred when  $\tau \sim 0.1 \text{ N m}^{-2}$  and  $W = 0.8$ , indicating  
5 that the winds were strong enough to perturb the pycnocline and stop the damping process  
6 (Fig. 9c).

7

## 8 **5.1 Internal seiche damping**

9

10 The wind stress changed from a state where  $\tau$  was strong enough to actively disturb the  
11 pycnocline ( $W < 1$ ) to a period of nearly calm winds ( $W > 1$ ) between the 16 and 24 August  
12 2008 (Fig. 9). During this period, both the along-fjord currents and temperatures tended to  
13 decay, which is clearly evident in the isolines of these properties at the three sites (Fig. 9).

14

15 To study the damping process in detail, we selected the time series of the along-fjord  
16 currents at a depth of 3 m at Cochamo during the above period in August to span the period  
17 of forcing, damping and re-enforcing of the internal oscillation.

18

19 Typically, any real oscillations undergo damping, which is given by the equation,

$$20 \quad x(t) = A e^{(-k t)} \cos(\omega t + \phi) \quad (7)$$

21 where  $t$  is time and  $A$  is the initial amplitude,  $k$  is the scale,  $\omega = 2\pi/T_N$  and  $\phi$  is the phase. In  
22 the case studied here,  $\phi = 0$ ,  $A = 8 \text{ cm s}^{-1}$ , and  $T_N = 2.5$  days, which was the internal period at  
23 Cochamo (Fig. 4). The best fit occurred when  $k = 1/3$  (Fig. 10).

24

25 The time for the initial amplitude  $A$  to decay to  $A \sim 0$  is the damping time ( $T_d$ ). There was a  
26 good fit (Fig. 10) between the observed current and the curve adjusted with the damping  
27 effect. Here,  $T_d = 9.1$  days, which is more than 3 times longer than the natural oscillation  
28 ( $T_N$ ); more precisely,  $T_d = 3.6 T_N$  at this site. The observed internal oscillations of the currents  
29 were not completely damped because the winds increased from nearly calm ( $W > 1$ ) to  
30 moderate conditions, which disturbed the pycnocline ( $W \sim 1$ ) and induced the intense



1 oscillations during the spring (Fig. 6). In the spring, the winds displayed a marked diurnal  
2 cycle that remained during the spring and summer (Castillo et al., 2012). This finding  
3 suggests that the internal seiche (mode 1) process is active without damping because it is  
4 forced daily (Fig. 3). Our findings indicated that the internal seiche process is an active  
5 contributor for the mixing in the Reloncavi fjord, the magnitude of this contribution might be  
6 similar as the tidal forcing. The maximum amplitude of the tidal currents on the Reloncavi  
7 fjord is  $10 \text{ cm s}^{-1}$  (Valle-Levinson et al., 2007; Castillo et al., 2012), taken the eq. 7 to  
8 estimate the maximum contribution of the tide obtain  $5 \times 10^{-3} \text{ m}^2 \text{ s}^{-2}$  which is similar to the  
9 observed  $K_E$  at the mouth (Fig. 7). One example of the dissipation of the energy through this  
10 process was observed previous to 19 August 2008 (Fig. 10), on there the maximum currents  
11 were  $0.7 \text{ m s}^{-1}$  and through eq. 7, we obtain  $K_E = 7 \times 10^{-3} \text{ m}^2 \text{ s}^{-2}$  great part of this energy  
12 might be dissipated within the Reloncavi fjord on 9 days. Future studies should focus on  
13 evaluating more precisely the available energy for the mixing process within the fjord and  
14 their effects on other water properties such as the salinity, oxygen or nutrients.

15

## 16 **6 Conclusions**

17

18 The along-fjord seasonal density structure of the Reloncavi fjord showed small changes in  
19 the stratification. The upper layer presents a persistent stratification from the surface to the  
20 pycnocline base, the latter of which has a mean depth of 2 m near the mouth and 6 m near the  
21 head of the fjord.

22

23 The along-fjord sealevel signal showed a 1.3 h energetic peak not related with any tidal  
24 harmonics, additionally at this period the sealevel amplitude at the mouth was significantly  
25 higher than the sealevel at the head of the fjord. This pattern was consistent with the presence  
26 of a barotropic seiche on the Reloncavi fjord.

27

28 The local winds stress was able to perturb the along-fjord pycnocline and produce internal  
29 seiche oscillations. The period centered on 3 days was consistent with the first baroclinic  
30 oscillation mode. This mode explained 44% of the variability of the 3 days band. The



1 oscillation was highly coherent along the fjord and with a phase nearly to  $0^\circ$ , consistent with  
2 a standing wave, like an internal seiche, within the Reloncavi fjord.

3

4 The internal seiche could be high contributor to the internal mixing within the fjord, in fact  
5 the kinetic energy ( $K_E$ ) associated to the internal seiche was similar to the maximum  
6 contribution of the tides in the along-fjord currents. During winter, the internal oscillations  
7 were present a relatively long period of time with nearly calm winds permit the estimation of  
8 the damping time of the internal seiche which was of 9 days, otherwise during the spring  
9 daily winds continuously forced the pycnocline.

10

#### 11 **Data availability**

12

13 The installation of the moorings for measuring the current, temperature and sealevel in the  
14 region was approved by the Chilean Navy through permit DS711. No specific permits were  
15 required to install the meteorological station because the location is a publicly controlled site.  
16 This study also did not involve any endangerment to species in the region. The authors  
17 indicated that all data are available to download from a COPAS-SUR Austral website  
18 (<http://www.reloncavi.udec.cl/>, last access 6 June 2016). The discharge data from the rivers  
19 of Chile are available from the Dirección General del Aguas de Chile website  
20 (<http://dgasatel.mop.cl/>, last access 1 July 2016). Also, all data sets can be requested from the  
21 corresponding author (Manuel I. Castillo).

22

#### 23 **Acknowledgements**

24 The authors thank the students (from Chile and Sweden) and technicians of the Physical  
25 Oceanography group of the Universidad de Concepcion who collaborated in performing the  
26 field measurements. This study is part of the PFB/31 COPAS-Sur Austral program and  
27 Centro de Investigación en Ecosistemas de la Patagonia by FIP2007-21 and Comité  
28 Oceanográfico Nacional CIMAR-CONA C17F 1107. Manuel I. Castillo was supported by  
29 FONDECYT grant no. 3130639 and by CONICYT-PAI no. 791220005.

30



## 1 References

- 2
- 3 Arneborg, L., and B. Liljebladh.: The internal seiches in Gullmar fjord part I -dynamics.  
4 Journal of Physical Oceanography **31**: 2549-2566, 2001a.
- 5 Arneborg, L., and B. Liljebladh: The internal seiches in Gullmar fjord part II - contribution  
6 to basin water mixing. Journal of Physical Oceanography **31**: 2567-2574, 2001b.
- 7 Cáceres, M., A. Valle-Levinson, H. Sepúlveda, and K. Holderied: Transverse variability of  
8 flow and density in a Chilean fjord. Continental Shelf Research **22**: 1683–1698,  
9 2002.
- 10 Castillo, M. I., O. Pizarro, U. Cifuentes, N. Ramirez, and L. Djurfeldt: Subtidal dynamics in  
11 a deep fjord of southern Chile. Continental Shelf Research **49**: 73-89, 2012.
- 12 Castillo, M. I., U. Cifuentes, O. Pizarro, L. Djurfeldt, and M. Caceres: Seasonal hydrography  
13 and surface outflow in a fjord with a deep sill: the Reloncaví fjord, Chile. Ocean Sci.  
14 **12**: 533-544, 2016.
- 15 COPAS-Sur Austral: Oceanografía del fiordo Reloncaví, Universidad de Concepción,  
16 available at: <http://www.reloncavi.udec.cl/>, last access 6 June 2016, 2012.
- 17 Cossu R, Wells MG. The Interaction of Large Amplitude Internal Seiches with a Shallow  
18 Sloping Lakebed: Observations of Benthic Turbulence in Lake Simcoe, Ontario,  
19 Canada, PLOS ONE doi: 10.1371/journal.pone.0057444, 2013.
- 20 Dirección General de Aguas: Datos hidrológicos en tiempo real, Chile, available at:  
21 <http://dgasatel.mop.cl/>, last access 1 July 2016, 2016.
- 22 Djurfeldt, L.: On the response of the Fjord Gullmaren under ice cover, J. of Geophys. Res.,  
23 **92**, 5157-5167, doi: 10.1029/JC092iC05p05157, 1987.
- 24 Dyer, K. R.: Estuaries: A Physical Introduction, John Wiley and Sons Inc, 140 pp., UK,  
25 1997.
- 26 Emery, W. J., and Thomson, R. E.: Data Analysis Methods in Physical Oceanography, 634  
27 pp., Elsevier, New York, USA, 1998.
- 28 Farmer, D. M., and Freeland, H. J.: The physical oceanography of Fjords. Prog. in  
29 Oceanogr., **12**, 147-194, doi: 10.1016/0079-6611(83)90004-6, 1983.
- 30 Farmer, D. M., and Smith, J.: Tidal interaction of stratified flow with a sill in Knight Inlet.  
31 Deep Sea Research Part A. Oceanographic Research Papers, **27**, 239-254, doi:  
32 10.1016/0198-0149(80)90015-1, 1980.
- 33 Gill, A.: Atmosphere-Ocean Dynamics, Academic Press, 662 pp., USA, 1982.
- 34 Goudsmit, G.-H., Burchard, H., Peeters, F. and Wüest, A.: Application of  $k-\epsilon$  turbulence  
35 models to enclosed basins: The role of internal seiches, J. Geophys. Res., **107**, 3230,  
36 doi: 10.1029/2001JC000954, 2002.
- 37 Grinsted, A., Moore, J. C., and Jevrejeva, S.: Application of the cross wavelet transform and  
38 wavelet coherence to geophysical time series, Nonlin. Processes Geophys., **11**, 561-  
39 566, doi:10.5194/npg-11-561-2004, 2004.
- 40 Inall, M. E., and Rippeth, T. P.: Dissipation of Tidal Energy and Associated Mixing in a  
41 Wide Fjord, Environmental Fluid Mechanics, **2**, 219-240, doi:  
42 10.1023/A:1019846829875, 2002.
- 43 Iriarte, J. L., Pantoja, S., and Daneri, G.: Oceanographic Processes in Chilean Fjords of  
44 Patagonia: from small to large-scale studies, Prog. in Oceanogr., **129**, 1-7, doi:  
45 10.1016/j.pocean.2014.10.004, 2014.
- 46



- 1 Large, W. G., and Pond, S.: Open-ocean momentum flux measurements in moderate to  
2 strong winds, *J. Phys. Oceanogr.*, 11, 324-336, 1981.
- 3 Lemmin, U.: The structure and dynamics of internal waves in Baldeggersee, *Limnol.*  
4 *Oceanogr.*, 32, 43-61, doi: 10.4319/lo.1987.32.1.0043, 1987.
- 5 León-Muñoz, J., Marcé, R., and Iriarte, J. L.: Influence of hydrological regime of an Andean  
6 river on salinity, temperature and oxygen in a Patagonia fjord, Chile, *New Zeal. J.*  
7 *Mar. Fresh.*, 47, 515–528, doi: 10.1080/00288330.2013.802700, 2013.
- 8 Letelier, J., Soto-Mardones, L., Salinas, S., Osuna, P., López, D., Sepúlveda, H. H., Pinilla,  
9 E., and Rodrigo, C.: Variabilidad del viento, oleaje y corrientes en la región norte de  
10 los fiordos Patagónicos de Chile, *Revista de Biología Marina y Oceanografía*, 46,  
11 363-377. . 2011.
- 12 Mans, C., Bramato, S., Baquerizo, A., and Losada, M.: Surface Seiche Formation on a  
13 Shallow Reservoir in Complex Terrain, *J. Hydraul. Eng-Asce*, 137, 517-529, 2011.
- 14 Maas, L. R. M., and Lam, F.-P. A.: Geometric focusing of internal waves, *J. of Fluid Mech.*,  
15 300, 1–41, doi: 10.1017/S0022112095003582, 1995.
- 16 Monismith, S.: An experimental study of the upwelling response of stratified reservoirs to  
17 surface shear stress, *J. of Fluid Mech.*, 171, 407-439, doi:  
18 10.1017/S0022112086001507, 1986.
- 19 Montero, P., Daneri, G., Gonzalez, H., Iriarte, J. L., Tapia, F.J., Lizarraga, L., Sanchez, N.,  
20 and Pizarro, O.: Seasonal variability of primary production in a fjord ecosystem of  
21 the Chilean Patagonia: Implications for the transfer of carbon within pelagic food  
22 webs, *Cont. Shelf Res.*, 31, 202-215, doi: 10.1016/j.csr.2010.09.003, 2011.
- 23 Mortimer, C. H.: Water movements in lakes during summer stratification; evidence from  
24 distribution of temperature in Windermere, *Phil. Trans. Roy. Soc. London*, 236, 355-  
25 404, doi : 10.1098/rstb.1952.0005, 1952.
- 26 Münnich, M., Wuest, A., and Imboden, D. M.: Observations of the 2nd Vertical-Mode of the  
27 Internal Seiche in an Alpine Lake, *Limnol. Oceanogr.*, 37, 1705-1719, doi:  
28 10.4319/lo.1992.37.8.1705, 1992.
- 29 Niemeyer, H. & P. Cereceda.: *Hidrografía. Geografía de Chile*, Tomo VIII, Instituto  
30 Geográfico Militar, Chile, 320 pp., 1984.
- 31 Palma, S., and Silva, N.: Distribution of siphonophores, chaetognaths, euphausiids and  
32 oceanographic conditions in the fjords and channels of southern Chile, *Deep-Sea Res.*  
33 *Pt. II*, 51, 513-53, doi:10.1016/j.dsr2.2004.05.001, 2004.
- 34 Pantoja, S., Iriarte, J. L., and Daneri, G.: Oceanography of the Chilean Patagonia, *Cont. Shelf*  
35 *Res.*, 31, 149-153, doi: 10.1016/j.csr.2010.10.013, 2011.
- 36 Parsmar, R., and Stigebrandt, A.: Observed damping of barotropic seiches through baroclinic  
37 wave drag in the Gullmar Fjord, *J. Phys. Oceanogr.*, 27, 849-857, 1997.
- 38 Pawlowicz, R.: Observations and linear analysis of sill-generated internal tides and estuarine  
39 flow in Haro Strait, *J. Geophys. Res-Oceans*, 107, doi: 10.1029/2000JC000504, 2002.
- 40 Pickard, G. L.: Some Physical Oceanographic Features of Inlets of Chile, *Journal of the*  
41 *Fisheries Research Board of Canada*, 28, 1077-1106, 1971.
- 42 Rabinovich, A.: Seiches and Harbor Oscillations, in: *Handbook of Coastal and Ocean*  
43 *Engineering*, Y. Kim (ed.), World Scientific Publishing Co, United States, 193-236,  
44 2010.
- 45





- 1 Ross L., Pérez-Santos, I., Valle-Levinson, A., Schneider, W.: Semidiurnal internal tides in a  
2 Patagonian fjord, *Prog. in Oceanogr.*, 129, 19-34, doi: 10.1016/j.pocean.2014.03.006,  
3 2014.
- 4 Schneider, W., Pérez-Santos, I., Ross, L., Bravo, L., Seguel, R. and Hernández, F.: On the  
5 hydrography of Puyuhuapi Channel, Chilean Patagonia. *Prog. in Oceanogr.*, 129, 8–  
6 18, doi: doi:10.1016/j.pocean.2014.03.007, 2014.
- 7 Simpson, J. H., Wiles P. J., and Lincoln, B. J.: Internal seiche modes and bottom boundary-  
8 layer dissipation in a temperate lake from acoustic measurements, *Limnol.*  
9 *Oceanogr.*, 56, 1893-1906, 2011
- 10 Stevens, C., Imberger, J.: The initial response of a stratified lake to a surface shear stress, *J.*  
11 *of Fluid Mech.*, 312, 39-66, doi: 10.1017/S0022112096001917, 1996.
- 12 Stigebrandt, A.: Vertical diffusion driven by internal waves in a sill Fjord, *J. Phys. Oceanogr.*  
13 6, 486-495, 1976.
- 14 Stigebrandt, A.: Some aspects of tidal interaction with fjord constrictions, *Estuarine and*  
15 *Coastal Marine Science*, 11, 151-166, doi: 10.1016/S0302-3524(80)80038-7, 1980
- 16 Stigebrandt, A., and Aure, J.: Vertical Mixing in Basin Waters of Fjords, *J. Phys. Oceanogr.*,  
17 917-926, 1989.
- 18 Svendsen, H.: Exchange processes above sill level between fjords and coastal water, in *Fjord*  
19 *Oceanography*, H. Freeland, Farmer, D. and Levings C. (eds.), Plenum Press, USA,  
20 355-361, 1980.
- 21 Thompson, R. O. R. Y., and Imberger J.: Response of a numerical model of a stratified lake  
22 to a wind stress, in *Proceedings of the 2nd International Symposium on Stratified*  
23 *Flows*, Trondheim, Norway, 24-27 June 1980, 562-570, 1980.
- 24 Thorpe, S.: Near-resonant forcing in a shallow two-layer fluid: a model for the internal surge  
25 in Loch New?, *J. of Fluid Mech.*, 63, 509-527, doi: 10.1017/S0022112074001753,  
26 1974.
- 27 Torrence C., and Compo, G.P.: A practical guide to wavelet analysis, *B. Am. Meteorol. Soc.*,  
28 79, 61-78, 1998.
- 29 Valle-Levinson, A., Sarkar, N., Sanay, R., Soto, D., and León, J.: Spatial structure of  
30 hydrography and flow in a Chilean fjord, *Estuario Reloncaví, Estuaries and Coasts*,  
31 30, 113-126, doi: 10.1007/BF02782972, 2007.
- 32 Valle-Levinson, A., Blanco, J. L., and Frangópulos, M.: Depth-dependent overtides from  
33 internal tide reflection in a glacial fjord, *Estuaries and Coasts*, 30: 127-136, 2007.
- 34 van der Lee E.M., and Umlauf, L.: Internal wave mixing in the Baltic Sea: Near-inertial  
35 waves in the absence of tides, *J. Geophys. Res-Oceans*, 116, C10016, doi:  
36 10.1029/2011jc007072, 2011.
- 37 Watson, E. R.: Movements of the waters of Loch Ness, as indicated by temperature  
38 observations, *The Geographical Journal*, 24, 430-437, doi: 10.2307/1775951, 1904.
- 39 Weddernburn, E. M.: An experimental investigation of the temperature changes occurring in  
40 fresh-water lochs, *Proc. R. Soc. Edinb.*, 28, 2-20, doi: 10.1017/S0370164600011524,  
41 1907.
- 42 Weddernburn, E. M. and Young, A.: Temperature observations in Loch Earn. Part II, *Trans.*  
43 *R. Soc. Edinb.*, 50, 741-767, doi: 10.1017/S0080456800017026, 1915.
- 44 Wiegand, R. C., and Chamberlain, V.: Internal waves of the second vertical mode in a  
45 stratified lake, *Limnol. Oceanogr.*, 32, 29-42, 1987.
- 46



1 **Figure captions**

2 **Figure 1:** Study region and location of the measuring stations. Left insert shows the area of  
3 the Reloncavi fjord (A). The location of the Reloncavi sound (B) is also shown. The right  
4 insert shows the study area (close-up view of A) and the positions of all measurements.  
5 Numbers are CTD stations.

6  
7 **Figure 2:** Seasonal profiles of density and bathymetry of the region. The upper inserts show  
8 the seasonal mean density profiles in each sub-basin of the fjord (a-d). In the insert below  
9 (e.), the along-fjord bathymetry and sub-basin nomenclature are shown. The black line  
10 represents the mean pycnocline depth, and corresponding standard deviations are represented  
11 by the gray shading.

12  
13 **Figure 3:** a) Along-fjord wind stress, positive up to the fjord; (b) sealevel, (c) Puelo river  
14 discharge, where the straight line represents the long-term mean and contours of along-fjord  
15 currents at (d) Cochamo, (e) Puelo and (f) the mouth. In the filled contours, the blue (red)  
16 colors indicate a net outflow (inflow).

17  
18 **Figure 4:** Spectra of along-fjord currents (above) at the mouth (a), Puelo (b) and Cochamo  
19 (c). Here black line indicate the averaged spectra for the upper layer (depths  $\leq h_1$ ) whereas  
20 gray lines showed spectra for currents at depths  $> h_1$ . (d) sealevel spectra at the mouth (black  
21 line) and at Cochamo (gray). (e) wind stress spectra for their along-fjord (black) and cross-  
22 fjord (gray) components. At the bottom each panel the 95% of confidence intervals for 48, 24  
23 and 12 degrees of freedom are shown.

24  
25 **Figure 5:** The left insert shows mean density ( $\sigma_t$ ) within the sub-basins. The pannels to the  
26 right of these show the first 3 baroclinic  $\psi_n(z)$  modes and modal speeds obtained from the  
27 CSM analysis (normalized). Note that phase velocity is in [m s<sup>-1</sup>].

28  
29 **Figure 6.** Band-passed along-fjord currents. Contours of band-passed (70-90 h) along-fjord  
30 currents. Negative (positive) currents in blue (in red) imply an outflow (inflow). Note the  
31 dotted square at the middle of August it is zooming on figure 9.



1

2 **Figure 7.** Projected along-fjord currents and kinetic energy ( $K_E$ ). Here presented the 1 to 3  
3 modal projections of the along-fjord band-passed (60-100 h) currents at Cochamo and at the  
4 mouth. At the bottom, present the  $K_E$  estimated using the projected components at the mouth  
5 (red) and at the mouth (black).

6

7 **Figure 8.** Coherence and phase wavelet spectra. Time series of along fjord wind-stress (a),  
8 and coherence and phase wavelet spectra for the relation mouth/Puelo (b, c) and  
9 Puelo/Cochamo (d, e). In the contours, the thick black line indicates squared coherence  $\geq 0.6$ ,  
10 only the associated phases were present on the phase wavelet. The thick black curve is the  
11 influence cone for the wavelet estimations.

12

13 **Figure 9.** Time-series of along-fjord wind stress ( $\tau$ ) and contours of along-fjord currents ( $V$ )  
14 and temperatures ( $T$ ) at Cochamo, Puelo and the mouth. There are three states of wind stress  
15 based on the Wedderburn number ( $W$ ) with (a) strong  $W < 1$ , (b) weak  $W > 1$  and moderate  
16  $W \sim 1$  winds. Note that contours of the current ( $V$ ) and temperature ( $T$ ) for a given location  
17 are plotted together.

18

19 **Figure 10.** Damping signal in currents. During a period of weak winds ( $W > 1$ ) at Cochamo  
20 (16 to 24 August 2008). The band-pass currents at the 3m depth (black line) was compared  
21 with a damping oscillatory curve  $x(t) = A e^{-kt} \cos(\omega t + \phi)$  (gray line). The damping time ( $T_d$ )  
22 was 3.6 times longer than the fundamental internal period ( $T_N$ ).

23

24

25

26

27

28



1

2 **Table titles**

3

4 **Table 1:** Characteristic of Reloncavi fjord. The name, mean depth (H) and length (L) of each  
5 sub-basin and for the entire fjord are presented.

6

7 **Table 2:** Seasonal statistics of the descriptive parameters of the fjord. Here we present the  
8 mean depth of the upper layer ( $h_1$ ), and densities of the upper ( $\rho_1$ ) and deep layers ( $\rho_2$ ). In  
9 addition, the phase and modal velocities ( $c$ ) and theirs periods (T) estimated using the  
10 Reduced Gravity and Continuously Stratified models are shown.

11



1 **Table 1.**

<b>Sub-basin</b>	<b>Description</b>	<b>H [m]</b>	<b>L [km]</b>
I	mouth–Marimeli	440	14.0
II	Marimeli – Puelo	250	13.0
III	Puelo–Cochamo	200	17.5
IV	Cochamo–head	82	10.5
<b>Total</b>	<b>mouth -head</b>	<b>250</b>	<b>55</b>

2  
3  
4  
5  
6  
7  
8  
9  
10  
11  
12



1 **Table 2.**

2

<b>Reduced Gravity Model (RGM)</b>					
	$h_1$ [m]	$\rho_1$ [kg m <sup>-3</sup> ]	$\rho_2$ [kg m <sup>-3</sup> ]	$c$ [m s <sup>-1</sup> ]	$T$ [days]
<b>Winter</b>	4.60 ± 0.60	1009.72 ± 4.32	1024.62 ± 0.74	0.76 ± 0.01	3.37 ± 0.03
<b>Spring</b>	4.79 ± 0.53	1007.63 ± 5.32	1024.78 ± 0.62	0.87 ± 0.02	2.92 ± 0.03
<b>Summer</b>	4.68 ± 0.26	1008.77 ± 3.26	1024.78 ± 0.63	0.83 ± 0.01	3.07 ± 0.02
<b>Autumn</b>	4.05 ± 0.41	1009.90 ± 3.92	1024.95 ± 0.48	0.75 ± 0.01	3.38 ± 0.03

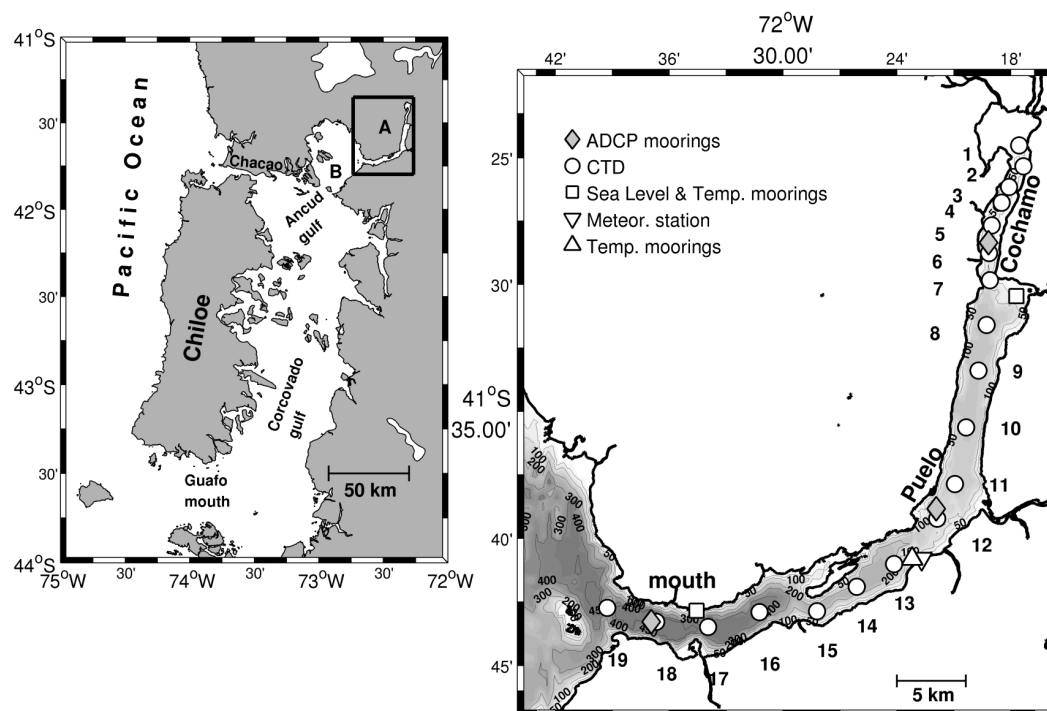
<b>Continuous Stratified Model (CSM)</b>						
	$c_1$ [m s <sup>-1</sup> ]	$c_2$ [m s <sup>-1</sup> ]	$c_3$ [m s <sup>-1</sup> ]	$T_1$ [days]	$T_2$ [days]	$T_3$ [days]
<b>Winter</b>	0.73 ± 0.11	1.46 ± 0.21	2.18 ± 0.32	3.50 ± 0.25	1.75 ± 0.13	1.17 ± 0.08
<b>Spring</b>	0.87 ± 0.10	1.73 ± 0.21	2.59 ± 0.31	2.94 ± 0.18	1.47 ± 0.09	0.98 ± 0.06
<b>Summer</b>	0.84 ± 0.07	1.68 ± 0.13	2.52 ± 0.20	3.03 ± 0.12	1.51 ± 0.06	1.01 ± 0.04
<b>Autumn</b>	0.77 ± 0.08	1.54 ± 0.15	2.32 ± 0.23	3.30 ± 0.16	1.65 ± 0.08	1.10 ± 0.05

3

4



1



2

3

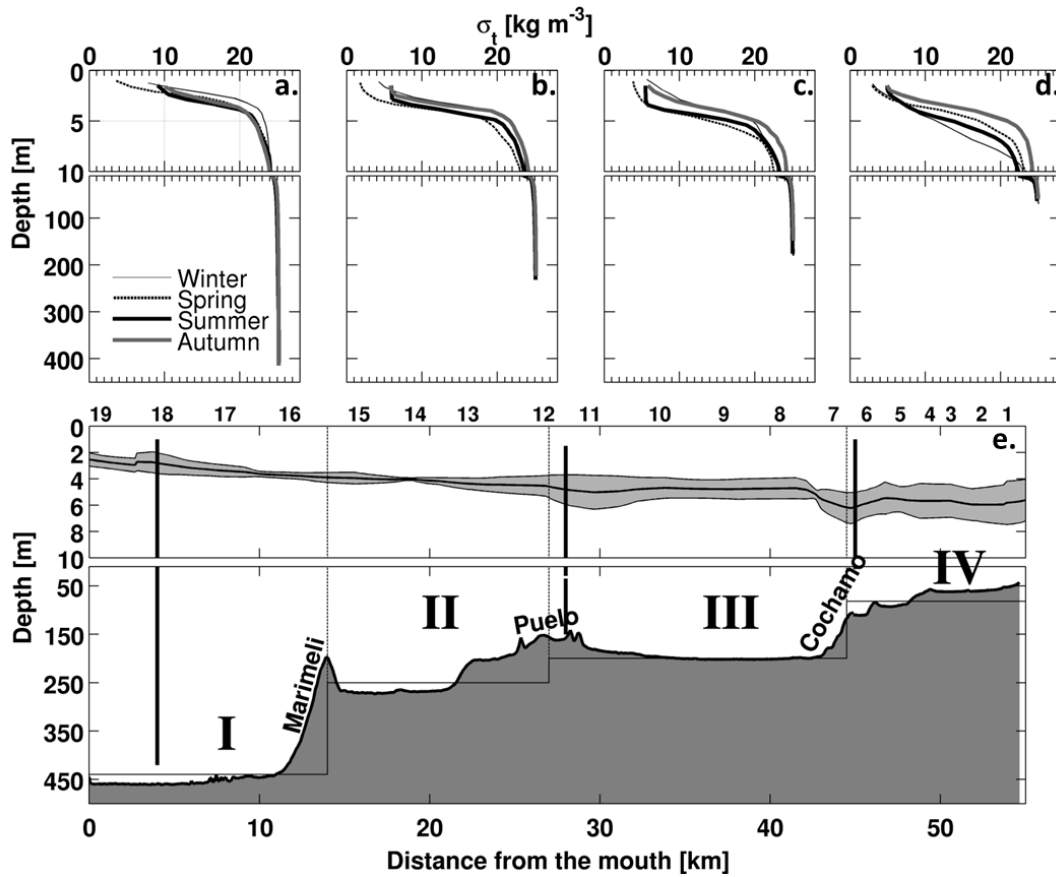
4 **Figure 1:** Study region and location of the measuring stations. Left insert shows the area of the  
5 Reloncavi fjord (A). The location of the Reloncavi sound (B) is also shown. The right insert  
6 shows the study area (close-up view of A) and the positions of all measurements. Numbers are  
7 CTD stations.

8

9



1



2

3

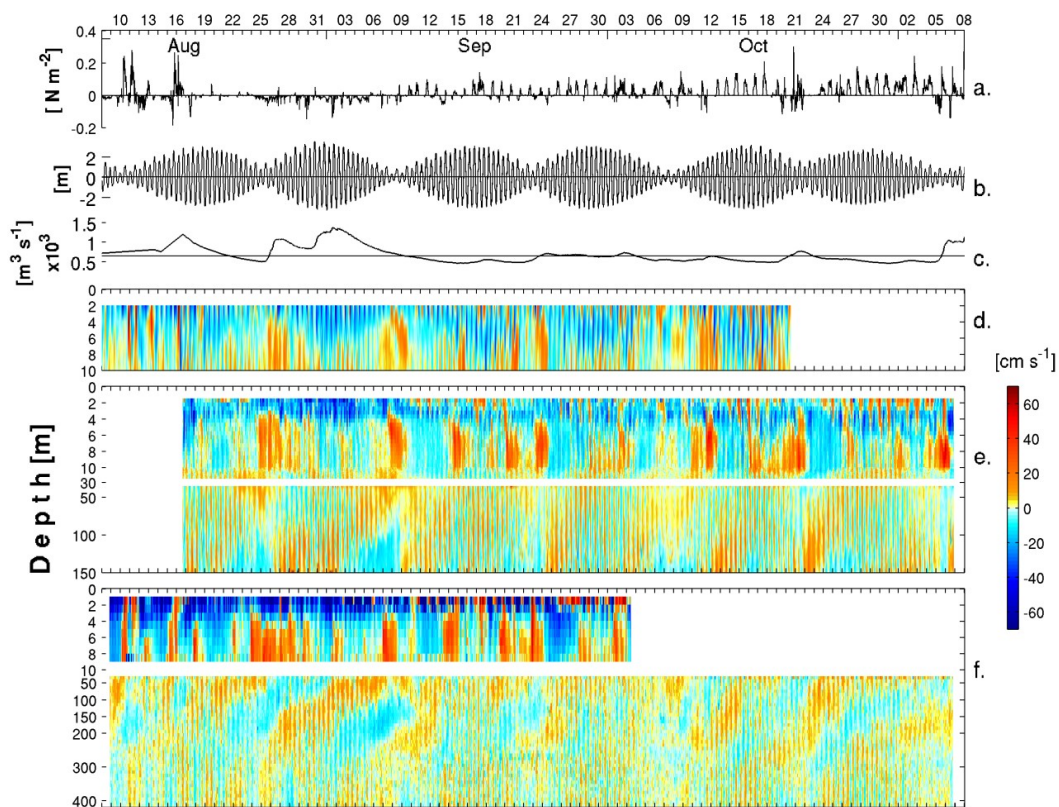
4 **Figure 2:** Seasonal profiles of density and bathymetry of the region. The upper inserts show the  
5 seasonal mean density profiles in each sub-basin of the fjord (a-d). In the insert below (e.), the  
6 along-fjord bathymetry and sub-basin nomenclature are shown. The black line represents the  
7 mean pycnocline depth, and corresponding standard deviations are represented by the gray  
8 shading.

9





1



2

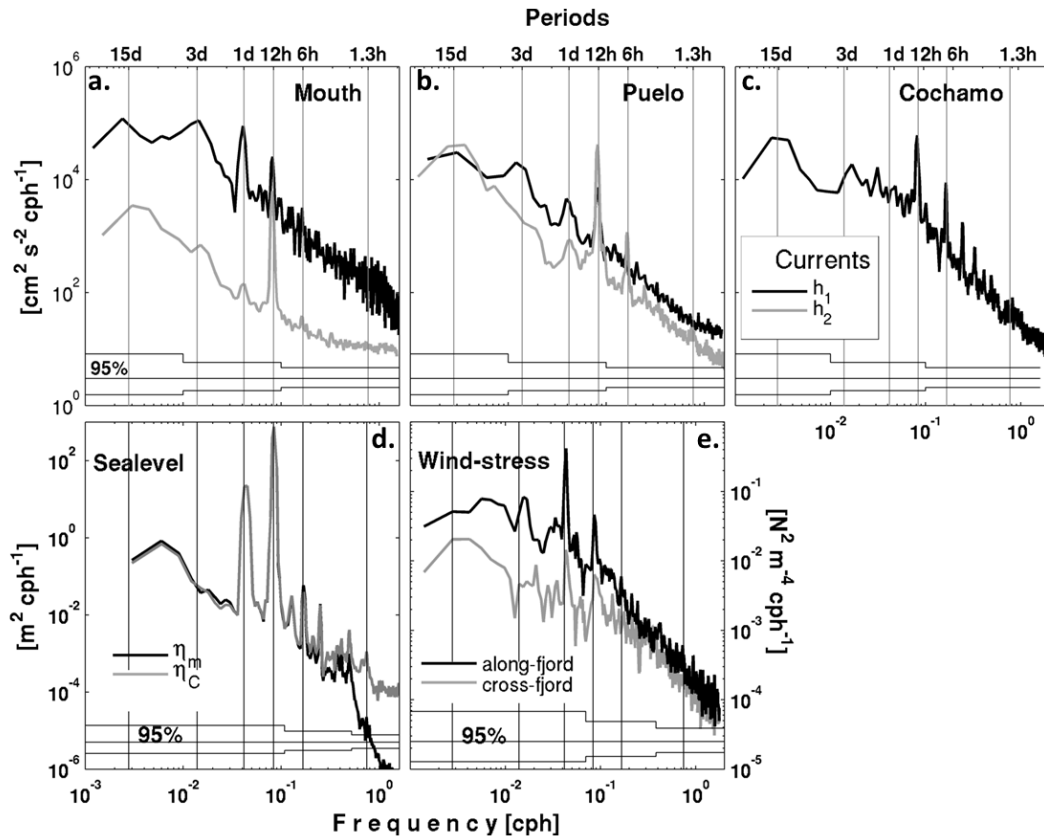
3

4 **Figure 3:** a) Along-fjord wind stress, positive up to the fjord; (b) sea level, (c) Puelo river  
5 discharge, where the straight line represents the long-term mean and contours of along-fjord  
6 currents at (d) Cochamo, (e) Puelo and (f) the mouth. In the filled contours, the blue (red)  
7 indicate a net outflow (inflow).

8



1



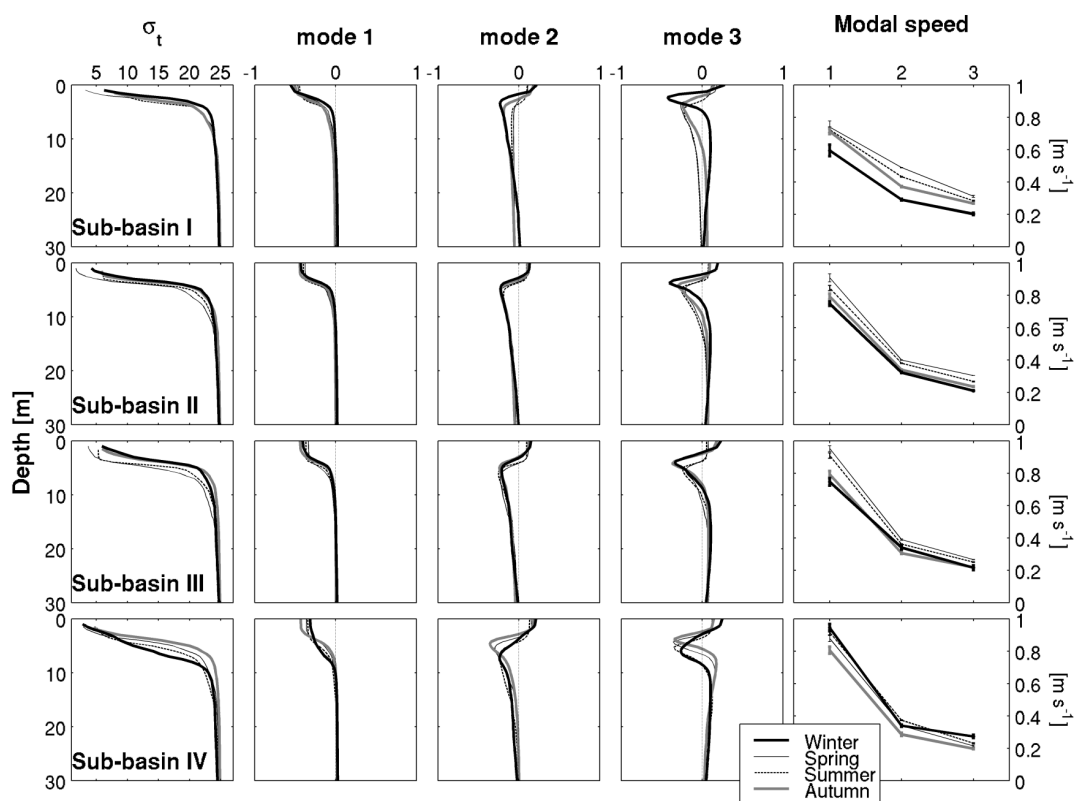
2

3 **Figure 4:** Spectra of along-fjord currents (above) at the mouth (a), Puelo (b) and Cochamo (c).  
 4 Here black line indicate the averaged spectra for the upper layer (depths  $\leq h_1$ ) whereas gray lines  
 5 showed spectra for currents at depths  $> h_1$ . (d) sealevel spectra at the mouth (black line) and at  
 6 Cochamo (gray). (e) wind stress spectra for their along-fjord (black) and cross-fjord (gray)  
 7 components. At the bottom each panel the 95% of confidence intervals for 48, 24 and 12 degrees  
 8 of freedom are shown.

9



1



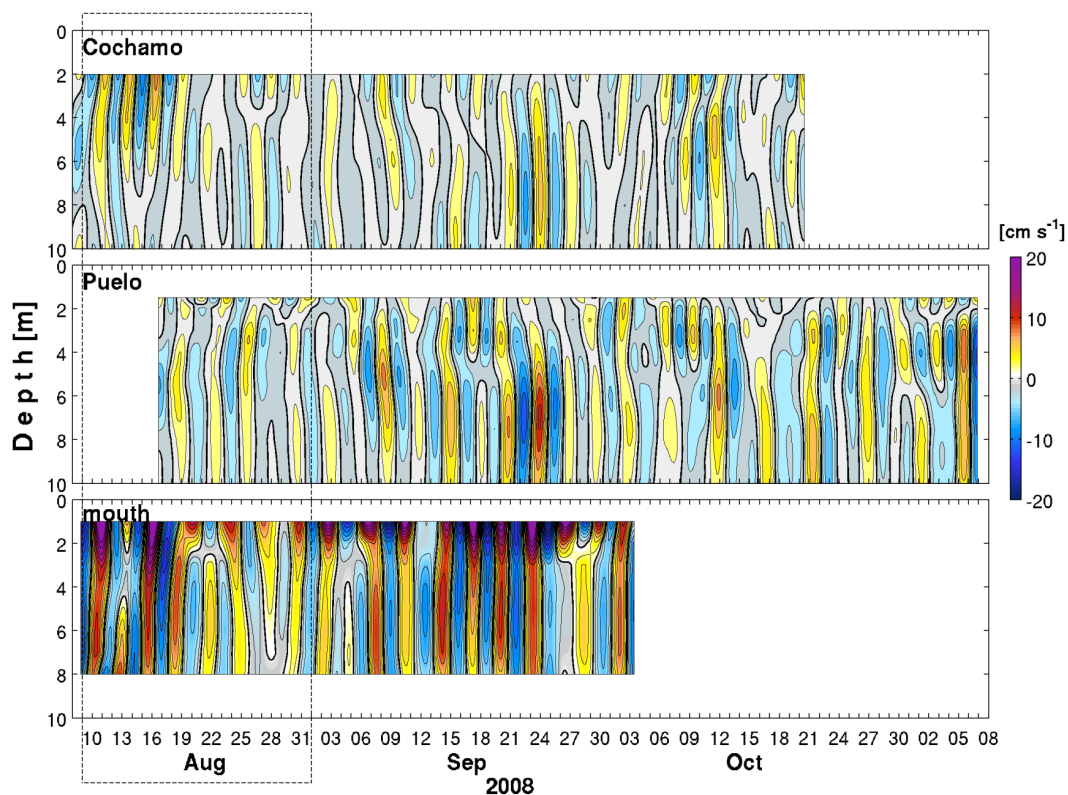
2

3 **Figure 5:** The left insert shows mean density ( $\sigma_t$ ) within the sub-basins. The panels to the right of  
 4 these show the first 3 baroclinic  $\psi_n(z)$  modes and modal speeds obtained from the CSM analysis  
 5 (normalized). Note that phase velocity is in [m s<sup>-1</sup>].

6



1



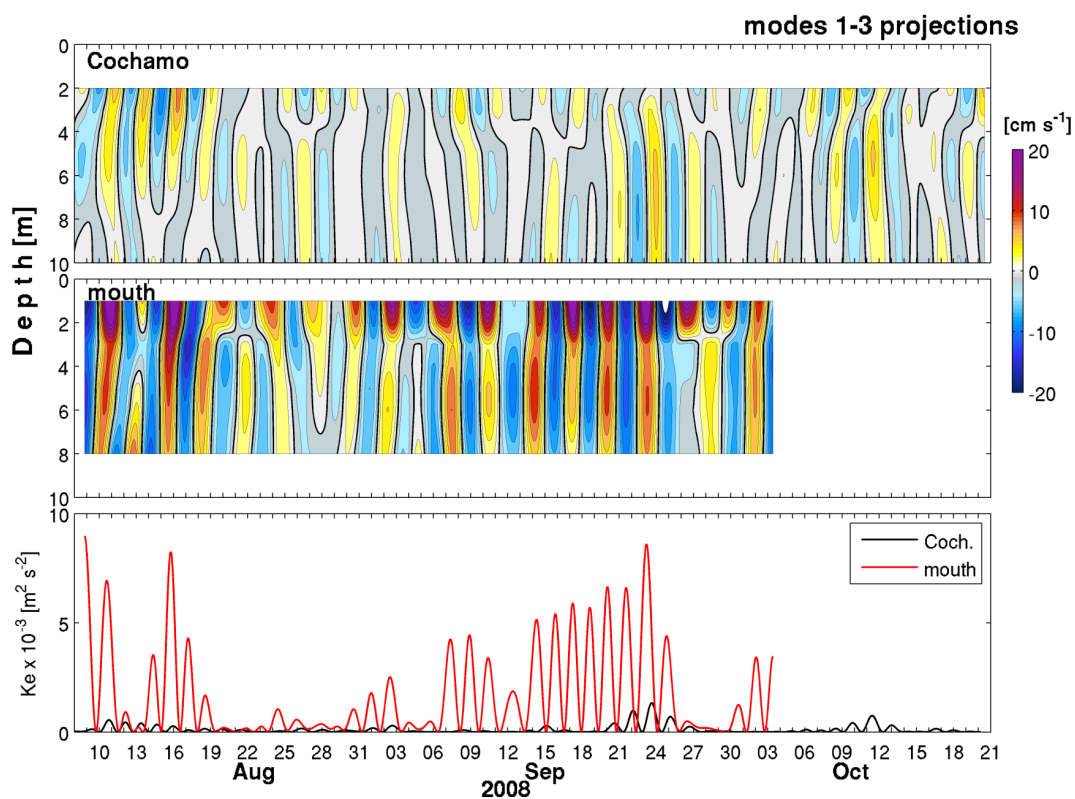
2

3 **Figure 6.** Band-passed along-fjord currents. Contours of band-passed (70-90 h) along-fjord  
4 currents. Negative (positive) currents in blue (in red) imply an outflow (inflow). Note the dotted  
5 square at the middle of August it is zooming on figure 9.

6



1



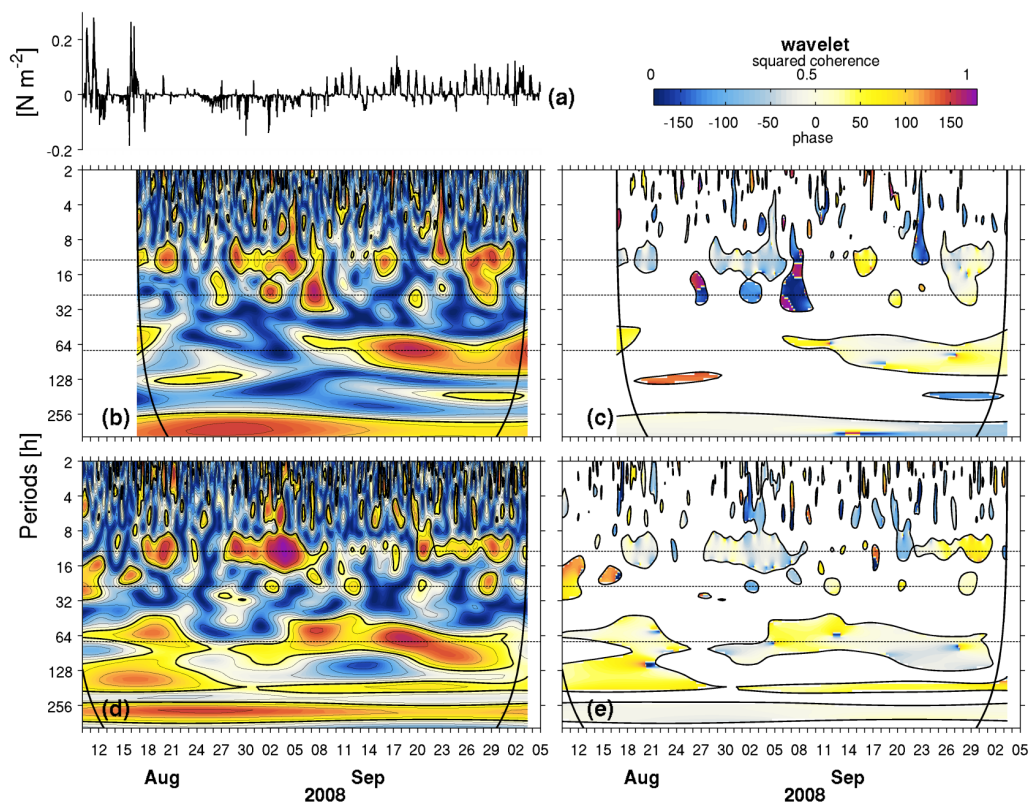
2

3 **Figure 7.** Projected along-fjord currents and kinetic energy ( $K_E$ ). Here presented the 1 to 3 modal  
4 projections of the along-fjord band-passed (60-100 h) currents at Cochamo and at the mouth. At  
5 the bottom, present the  $K_E$  estimated using the projected components at the mouth (red) and at the  
6 mouth (black).

7



1



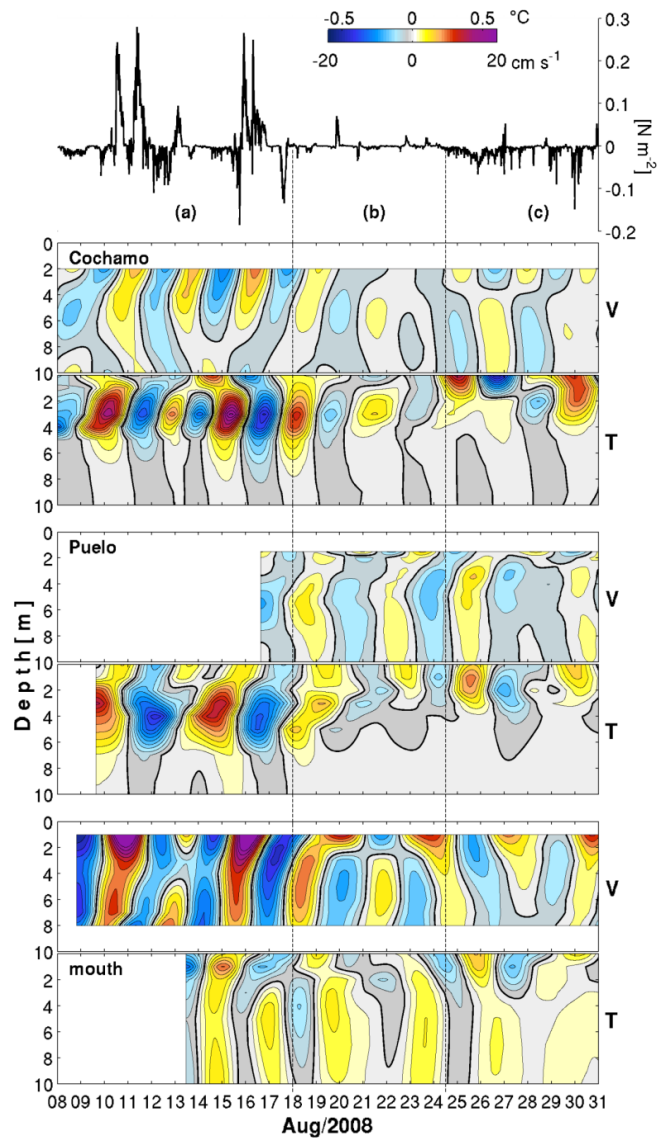
2

3 **Figure 8.** Coherence and phase wavelet spectra. Time series of along fjord wind-stress (a), and  
4 coherence and phase wavelet spectra for the relation mouth/Puelo (b, c) and Puelo/Cochamo (d,  
5 e). In the contours, the thick black line indicates squared coherence  $\geq 0.6$ , only the associated  
6 phases were present on the phase wavelet. The thick black curve is the influence cone for the  
7 wavelet estimations.

8



1

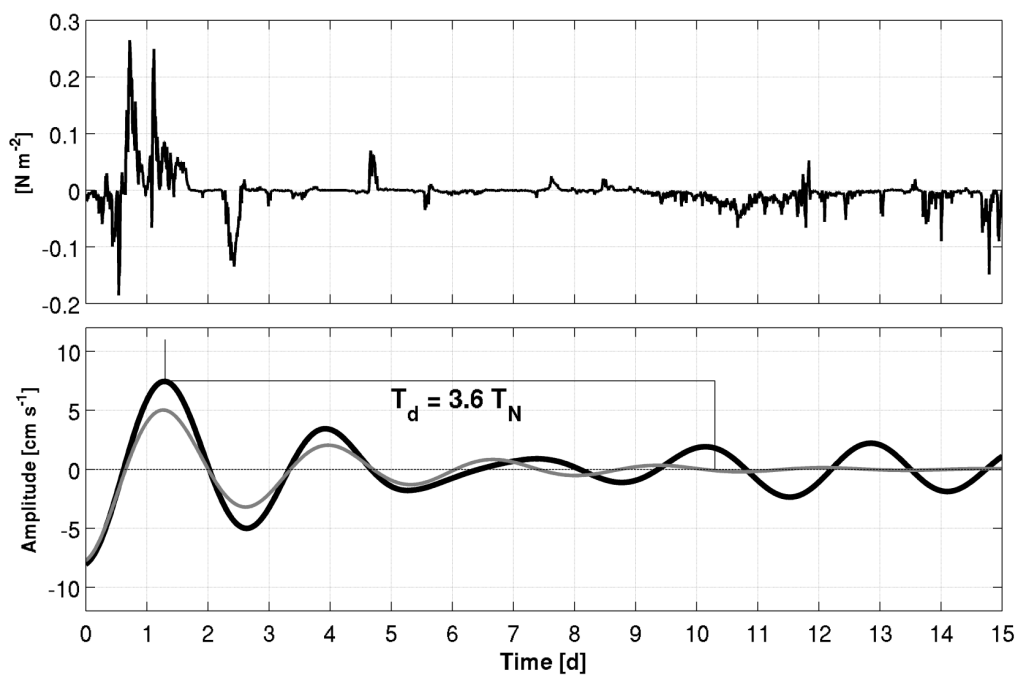


2

3 **Figure 9.** Time-series of along-fjord wind stress ( $\tau$ ) and contours of along-fjord currents (V) and  
4 temperatures (T) at Cochamo, Puelo and the mouth. There are three states of wind stress based on  
5 the Wedderburn number ( $W$ ) with (a) strong  $W < 1$ , (b) weak  $W > 1$  and moderate  $W \sim 1$  winds.  
6 Note that contours of the current (V) and temperature (T) for a given location are plotted  
7 together.



1



2

3 **Figure 10.** Damping signal in currents. During a period of weak winds ( $W > 1$ ) at Cochamo (16 to  
4 24 August 2008). The band-pass currents at the 3m depth (black line) was compared with a  
5 damping oscillatory curve  $x(t) = A e^{-kt} \cos(\omega t + \phi)$  (gray line). The damping time ( $T_d$ ) was 3.6  
6 times longer than the fundamental internal period ( $T_N$ ).

7

8